


RESEARCH ARTICLE

# High-efficiency inverse dynamics modeling of parallel posture alignment mechanism with actuation redundancy

Zhihao Wang<sup>1,2</sup> , Hongbin Li<sup>1,2</sup> and Nina Sun<sup>1,2</sup>

<sup>1</sup>College of Transportation, Ludong University, Yantai City, China and <sup>2</sup>College of Intelligent Manufacturing Industry, Ludong University, Yantai City, China

**Corresponding author:** Zhihao Wang; Email: [wangzhihao0312@foxmail.com](mailto:wangzhihao0312@foxmail.com)

**Received:** 2 November 2022; **Revised:** 6 April 2023; **Accepted:** 11 April 2023; **First published online:** 4 May 2023

**Keywords:** parallel mechanism; high efficiency; analytical modeling; inverse dynamics; actuation redundancy

## Abstract

The analytical expression of driving force is helpful to quickly plan the kinematic trajectory of parallel mechanism for automatic drilling and riveting. For parallel posture alignment mechanism, because of its closed-loop characteristics, the inverse dynamic solution is more complex, especially for parallel bracket with actuation redundancy. Considering that the telescopic rods are actually flexible parts, the dynamic analytical modeling is carried out with deformation supplementary equation. Taking the force at the spherical joint as the intermediate variable and the driving force of each active prismatic pair are analytically analyzed by vector cross-product. The modeling was verified by experiment. Compared with previous research methods, the analytical method proposed improves the solution accuracy of driving force slightly and reduces the driving force solution time by 56.28%, which is high efficiency. The maximum error percentage is 1.61%, and the experimental results show that the method of inverse dynamics modeling is practical. This paper can be used for driving force analysis of parallel posture alignment mechanism based on positioner in the field of aircraft assembly.

## 1. Introduction

Parallel mechanism with actuation redundancy can reduce the driving force of each prismatic pair under specified trajectory [1, 2]. However, the driving forces of parallel mechanism need to be allocated reasonably as a result of that unreasonable driving forces will lead to huge internal forces, damage or accidents. Moreover, driving force analysis is also the premise of trajectory planning. To analyze the driving force of the mechanism, dynamic modeling is needed. Dynamic modeling methods include Lagrange method, Newton–Euler method, virtual work principle, Kane equation method, and so on [3].

Newton–Euler method establishes the Newton equation and Euler equation of the analytic object separately and then solves the equation, which can calculate the force and moment between the motion pairs [4]. From the view of energy analysis, Lagrange method calculates the kinetic energy and potential energy of components. Then, the system variables are differentiated and Lagrange equation is established [5]. The principle of virtual work establishes dynamic equation based on that sum of virtual work done by active force and moment, inertia force and moment are equal to zero [6]. Kane equation method solves the unknown quantity by means of the equilibrium equation about the generalized velocity, partial velocity, active force and inertial force of the rigid body [7]. When carrying out deformation coordination analysis, it is necessary to calculate the forces between components at the spherical joint. Newton–Euler method can analyze the force between components, so Newton–Euler method is used for dynamic modeling. Therefore, the dynamic analysis of parallel posture alignment mechanism is carried out by Newton–Euler method.

Many scholars have used Newton–Euler method to study the dynamic modeling of parallel mechanisms [8]. Jiao et al. [9] studied the dynamics characteristics of 2-DOF planar parallel manipulator.

Jiang et al. [10] did similar research and the redundant driving force of parallel mechanism was optimized. Research object of the above article is a planar mechanism, whose dynamic analysis does not involve the solution of space force and moment, so it is less difficult to solve. Chen researched 4-UPS-UPU parallel mechanism and proposed corresponding dynamic model. However, the 4-UPS-UPU parallel mechanism is not a redundant drive parallel mechanism, and the dynamics modeling does not involve the supplement of constraint equation [11]. D–H method [12] can be used to drive the kinematic and dynamic equations, but researchers need to set up the coordinate system according to the D–H rule.

For parallel mechanisms with actuation redundancy, the number of constraint equations is less than that of the unknown quantity [13]. Therefore, it is necessary to supplement the constraint equation. Deformation compatibility analysis is required. For the parts of the mechanism, there is no infinite stiffness body and elastic deformation inevitably occurs under the function of internal forces [14]. For the parts used in automatic drilling and riveting system, because of the large area of aircraft panels and skin, the posture alignment mechanism has a longer span and a larger weight [15]. This will inevitably lead to elastic deformation of telescopic rod. Therefore, it is necessary to consider telescopic rod as a flexible body when dynamics modeling. Especially for parallel mechanism with actuation redundancy, the number of constraint equations is less than the number of unknown variables in dynamic modeling. It is necessary to increase the number of constraint equations by combining deformation compatibility equation [16]. When dynamic simulation analysis is carried out, the deformed parts need to be designed as flexible bodies [17]. Considering the influence of structural flexibility, Liu et al. conducted a dynamic modeling of active over-constrained parallel manipulator based on deformation coordination [18]. By combining equilibrium and deformation coordination equations, wang et al proposed dynamic model for a 7-DOF serial-parallel hybrid humanoid robotic arm [19].

The purpose of this paper is to establish the analytical solution of the driving force of the parallel posture alignment mechanism with actuation redundancy and improve the efficiency and accuracy of the driving force. The driving force solved in paper refers to the force required to act on prismatic pair with servo motor installed.

The remainder of this paper is organized as follows. The Section 2 introduces the structure, degree of freedom and working principle of the automatic drilling and riveting system composed of parallel posture alignment mechanism and end actuator. In the Section 3, the kinematics analysis is presented, mainly including the inverse solution of posture, velocity and acceleration. In the Section 4, the dynamics modeling is studied, and the analytical expression of driving force is derived. The Section 5 carries out simulation analysis, and the Section 6 conducts experimental verification.

## 2. Bracket type parallel posture alignment mechanism

The automatic drilling and riveting system shown in Fig. 1(a) is composed of parallel posture alignment mechanism whose structural diagram is shown in Fig. 1(d) and end actuator whose structural diagram is shown in Fig. 1(e). The PS-PPS-2PPPS parallel posture alignment mechanism consists of four positioners [20] and a moving platform. As shown in Fig. 1(b), the parallel posture alignment mechanism can translate along the  $z_b$  axis of the global coordinate system with distance  $z_i^b$ , rotate around the  $x_b$  axis and  $y_b$  axis of the global coordinate system with angle  $\alpha_i^b$  and  $\beta_i^b$ , respectively. The positioner 1 is equipped with  $x$  direction active prismatic pair which driven by motor. The positioner 2 is equipped with  $x$ - and  $z$ -direction active prismatic pair. The positioner 3 and 4 are equipped with  $x$ ,  $y$  and  $z$  direction prismatic pair, among which,  $z$  direction prismatic pair is active prismatic pair and the other ones are follow-up prismatic pair which do not have motor installed.

Global coordinate system  $O_b - x_b y_b z_b$ , moving platform coordinate system  $O_t - x_t y_t z_t$ , positioner coordinate system  $O_i - x_i y_i z_i$  and degree of freedom of parallel posture alignment mechanism are shown in Fig. 1(b).  $i$  represents the number of positioner. The direction of  $x$ ,  $y$  and  $z$  axis of the global coordinate system is from  $S_2$  to  $S_1$ ,  $S_1$  to  $S_4$  and  $O_b$  to  $S_1$ , respectively. Coordinate axis of positioner coordinate system are parallel to the ones of global coordinate system.  $O_b$  coincides with  $O_1$ .  $O_i$  is located at center

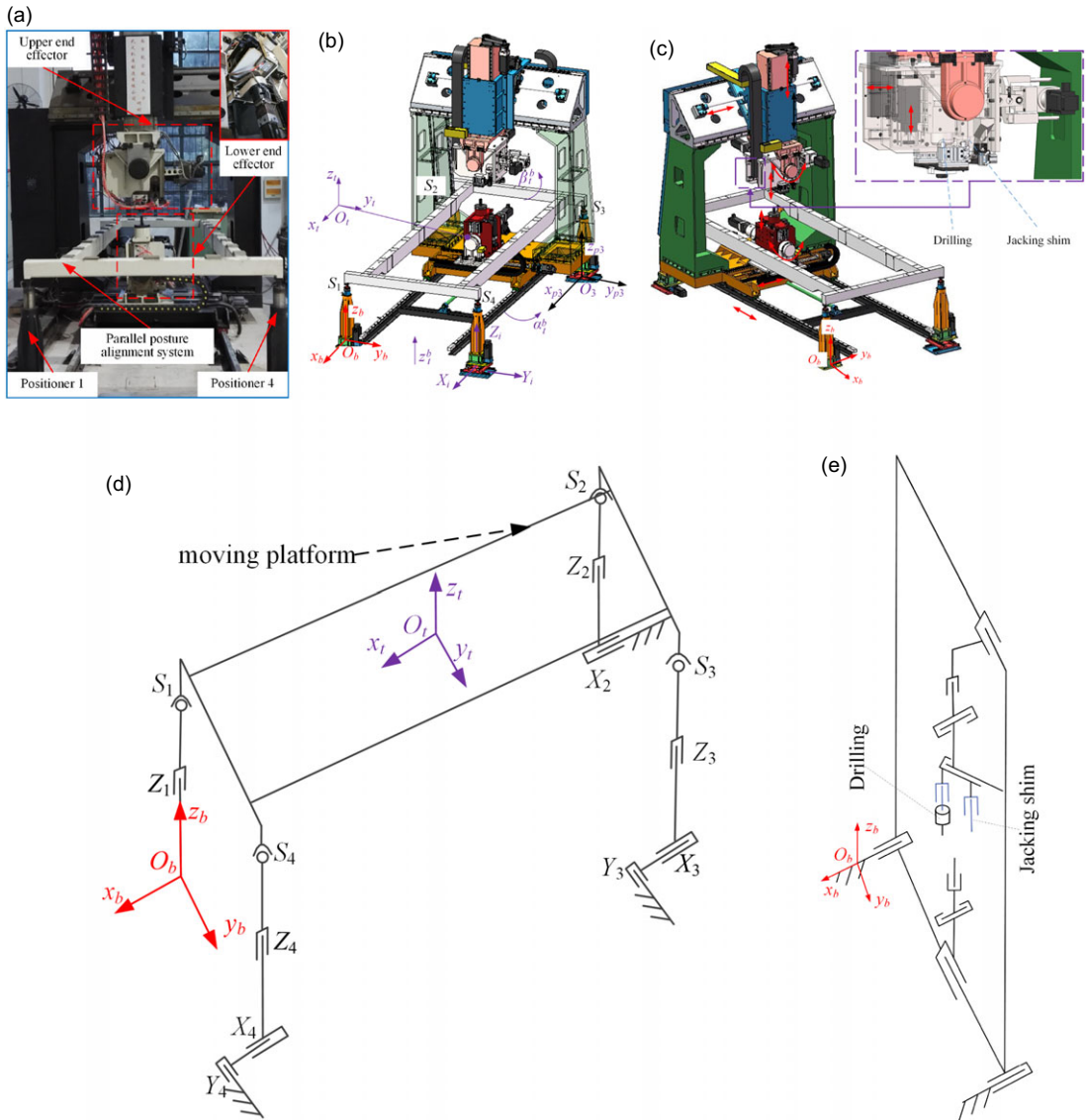


**Figure 1.** Automatic drilling and riveting machine. (a) Picture of real products. (b) Three-dimensional model. (c) Motion pair of end effector. (d) Structural diagram of parallel posture alignment mechanism. (e) Structural diagram of end effector.

of the upper plane of moving platform. Coordinate axis of moving platform coordinate system is parallel to the ones of global coordinate system at the beginning. When adjusting the parallel posture alignment mechanism, the moving platform firstly rotates around the  $x_b$  axis and then rotates around the  $y_b$  axis.  $X_i$ ,  $Y_i$  and  $Z_i$  denote prismatic pair of positioner and  $S_i$  denotes spherical joint connecting positioner and moving platform. Coordinate system origin of positioner 1~4 are located at  $Z_1 = 0$ ,  $X_2 = 0$ ,  $Y_3 = 0$ ,  $Y_4 = 0$ , respectively. The moving pair of the end actuator is shown in Fig. 1(c). The design accuracy of parallel posture alignment mechanism is 0.5 mm for position error and  $0.5^\circ$  for posture error.

Through offline programming, the motion path of the end effector and the parallel posture alignment mechanism is planned. Then, the pose of the parallel posture alignment mechanism and the end effector is adjusted for rough positioning. Precise positioning is carried out by laser ranging device and visual

imaging device. At last, the upper end actuator is used to drilling, and then, the upper end actuator and the lower end actuator are used for riveting.

### 3. Kinematics analysis of low DOF parallel mechanism

Kinematic analysis is the basis of dynamic analysis, which including pose inverse solution, velocity inverse solution and acceleration inverse solution of parallel posture alignment mechanism. First of all, it is necessary to analyze the relationship between the degree of freedom and the pose parameter of the mechanism. Kutzbach–Grüble formula [21] can be used to calculate the freedom of the parallel posture alignment mechanism, as shown in Eq. (1).

$$M = 6(n_m - g_m - 1) + \sum_{h=1}^{g_m} f_h = 6 \times (11 - 13 - 1) + 21 = 3 \tag{1}$$

where  $M$  represents the degree of freedom of the mechanism and  $n_m$  represents the number of parts.  $g_m$  represents the number of motion pairs.  $f_h$  represents the degrees of freedom of  $h$ th kinematic pair.

Therefore, only three components of the mechanism’s pose variables are independent, and the other variables should be determined according to independent variables. In other words, displacement of each prismatic pair is related to three independent variables in pose parameters  $(x_t^b, y_t^b, z_t^b, \alpha_t^b, \beta_t^b, \gamma_t^b)$ . The posture alignment parallel mechanism has no degree of freedom of rotation about the  $z_b$  axis of the global coordinate system. What’s more, according to Eq. (2),  $x_t^b$  and  $y_t^b$  can be calculated by  $\alpha_t^b$  and  $\beta_t^b$ .

$$\begin{aligned} x_t^b &= -\frac{l \cos \beta_t^b}{2} + \frac{w \sin \alpha_t^b \sin \beta_t^b}{2} + h \cos \alpha_t^b \sin \beta_t^b \\ y_t^b &= \frac{w \cos \alpha_t^b}{2} - h \sin \alpha_t^b \end{aligned} \tag{2}$$

where  $l$ ,  $w$  and  $h$  denote the distance between  $O_2$  and  $O_b$ ,  $O_2$  and  $O_3$ ,  $S_i$  and upper plane of moving platform, respectively. Therefore, the independent variables in pose parameters are  $(z_t^b, \alpha_t^b, \beta_t^b)$ .

#### 3.1. Inverse solution of pose

The inverse solution of pose establishes the mapping relationship between the posture parameters of moving platform and the displacement of prismatic pair in the local coordinate system. The posture transformation matrix of the parallel posture alignment mechanism is:

$$\mathbf{R}_t^b = \mathbf{R}(y_b, \beta_t^b) \mathbf{R}(x_b, \alpha_t^b) = \begin{bmatrix} \cos \beta_t^b & \sin \beta_t^b \sin \alpha_t^b & \sin \beta_t^b \cos \alpha_t^b \\ 0 & \cos \alpha_t^b & -\sin \alpha_t^b \\ -\sin \beta_t^b & \cos \beta_t^b \sin \alpha_t^b & \cos \beta_t^b \cos \alpha_t^b \end{bmatrix} \Bigg|_{\gamma_t^b=0} \tag{3}$$

where the posture alignment parallel mechanism has no degree of freedom of rotation about the  $z_b$  axis of the global coordinate system. As shown in Eq. (4), the displacement of each prismatic pair can be obtained by using space vector chain method:

$$\begin{aligned} d_i^x &= (\mathbf{R}_t^b \lambda_{si}^t + \mathbf{P}_t^b - \lambda_{oi}^b)^T \mathbf{n}^x \\ d_i^y &= (\mathbf{R}_t^b \lambda_{si}^t + \mathbf{P}_t^b - \lambda_{oi}^b)^T \mathbf{n}^y \\ d_i^z &= (\mathbf{R}_t^b \lambda_{si}^t + \mathbf{P}_t^b - \lambda_{oi}^b)^T \mathbf{n}^z \end{aligned} \tag{4}$$

where  $\mathbf{n}_x = [1, 0, 0]^T$ ,  $\mathbf{n}_y = [0, 1, 0]^T$  and  $\mathbf{n}_z = [0, 0, 1]^T$ .  $\mathbf{n}_x$ ,  $\mathbf{n}_y$  and  $\mathbf{n}_z$  denote the direction vector.  $\mathbf{P}_t^b = [x_t^b, y_t^b, z_t^b]^T$  denotes the vector of moving platform coordinate system origin  $O_t$  relative to global

coordinate system origin  $O_b$ .  $\lambda_{si}^t$  represents the vector of  $S_i$  relative to  $O_t$ . It can be calculated from Eq. (5) that the displacement of each prismatic pair of the positioner driven by servo motor is:

$$\begin{aligned}
 d_1^z &= -l \sin \beta_t^b / 2 - w \cos \beta_t^b \sin \alpha_t^b / 2 - h \cos \beta_t^b \cos \alpha_t^b + z_t^b \\
 d_2^x &= l - l \cos \beta_t^b \\
 d_2^z &= l \sin \beta_t^b / 2 - w \cos \beta_t^b \sin \alpha_t^b / 2 - h \cos \beta_t^b \cos \alpha_t^b + z_t^b \\
 d_3^z &= l \sin \beta_t^b / 2 + w \cos \beta_t^b \sin \alpha_t^b / 2 - h \cos \beta_t^b \cos \alpha_t^b + z_t^b \\
 d_4^z &= -l \sin \beta_t^b / 2 + w \cos \beta_t^b \sin \alpha_t^b / 2 - h \cos \beta_t^b \cos \alpha_t^b + z_t^b
 \end{aligned} \tag{5}$$

where  $d_i^z$  and  $d_i^x$  represent the relative displacement of prismatic pair in  $z$  and  $x$  direction, respectively.

### 3.2. Inverse solution of velocity

The inverse solution of pose establishes the mapping relationship between the generalized velocity of moving platform and the velocity of prismatic pair in the local coordinate system. Relative velocity of prismatic pair can be calculated as follow:

$$v_i^j = [\mathbf{v}_t^b + \omega_t^b \times (\mathbf{R}_t^b \lambda_{si}^t)] \cdot \mathbf{n}_i^j = [(\mathbf{n}_i^j)^T (\mathbf{R}_t^b \lambda_{si}^t \times \mathbf{n}_i^j)^T] \begin{bmatrix} \mathbf{v}_t^b \\ \omega_t^b \end{bmatrix} \tag{6}$$

where  $\mathbf{v}_t^b$  and  $\omega_t^b$  denote velocity and angular velocity of moving platform in global coordinate system, respectively. The velocity  $\mathbf{v}_t^b$  and angular velocity  $\omega_t^b$  of moving platform can be expressed as:

$$\omega_t^b = \mathbf{R}(y_b, \beta_t^b) \begin{bmatrix} 1 \\ 0 \\ 0 \end{bmatrix} \dot{\alpha}_t^b + \begin{bmatrix} 0 \\ 1 \\ 0 \end{bmatrix} \dot{\beta}_t^b = \begin{bmatrix} 0 & \cos \beta_t^b & 0 \\ 0 & 0 & 1 \\ 0 & -\sin \beta_t^b & 0 \end{bmatrix} \begin{bmatrix} \dot{z}_t^b \\ \dot{\alpha}_t^b \\ \dot{\beta}_t^b \end{bmatrix} \tag{7}$$

$$\mathbf{v}_t^b = \begin{bmatrix} 0 & \partial x_t^b / \partial \alpha_t^b & \partial x_t^b / \partial \beta_t^b \\ 0 & \partial y_t^b / \partial \alpha_t^b & 0 \\ 1 & 0 & 0 \end{bmatrix} \begin{bmatrix} \dot{z}_t^b \\ \dot{\alpha}_t^b \\ \dot{\beta}_t^b \end{bmatrix} \tag{8}$$

Therefore, the relationship between the speed of each prismatic pair and the generalized speed of moving platform can be expressed as:

$$\begin{bmatrix} v_1^z \\ v_2^x \\ v_2^z \\ v_3^x \\ v_3^y \\ v_3^z \\ v_4^x \\ v_4^y \\ v_4^z \end{bmatrix} = \begin{bmatrix} \mathbf{n}_z^T (\lambda_{s1}^b \times \mathbf{n}_z)^T \\ \mathbf{n}_x^T (\lambda_{s2}^b \times \mathbf{n}_x)^T \\ \mathbf{n}_z^T (\lambda_{s2}^b \times \mathbf{n}_z)^T \\ \mathbf{n}_x^T (\lambda_{s3}^b \times \mathbf{n}_x)^T \\ \mathbf{n}_y^T (\lambda_{s3}^b \times \mathbf{n}_y)^T \\ \mathbf{n}_z^T (\lambda_{s3}^b \times \mathbf{n}_z)^T \\ \mathbf{n}_x^T (\lambda_{s4}^b \times \mathbf{n}_x)^T \\ \mathbf{n}_y^T (\lambda_{s4}^b \times \mathbf{n}_y)^T \\ \mathbf{n}_z^T (\lambda_{s4}^b \times \mathbf{n}_z)^T \end{bmatrix} \begin{bmatrix} 0 & \frac{\partial x_t^b}{\partial \alpha_t^b} & \frac{\partial x_t^b}{\partial \beta_t^b} \\ 0 & \frac{\partial y_t^b}{\partial \alpha_t^b} & 0 \\ 1 & 0 & 0 \\ 0 & \cos \beta_t^b & 0 \\ 0 & 0 & 1 \\ 0 & -\sin \beta_t^b & 0 \end{bmatrix} \begin{bmatrix} \dot{z}_t^b \\ \dot{\alpha}_t^b \\ \dot{\beta}_t^b \end{bmatrix} \tag{9}$$

where  $v_i^x$ ,  $v_i^y$  and  $v_i^z$  represent the relative velocity of prismatic pair in  $x$ ,  $y$  and  $z$  direction, respectively.  $\lambda_{si}^b$  represents the vector of  $S_i$  relative to  $O_b$  which can be expressed as  $\lambda_{si}^b = \mathbf{R}_t^b \lambda_{si}^t$ .

### 3.3. Inverse solution of acceleration

The inverse solution of pose establishes the mapping relationship between the generalized acceleration of moving platform and the acceleration of prismatic pair in the local coordinate system. Relative acceleration of prismatic pair can be calculated according to Eq. (10):

$$a_i^j = [\dot{v}_i^b + \dot{\omega}_i^b \times \lambda_{si}^b + \omega_i^b \times (\omega_i^b \times \lambda_{si}^b)]^T \mathbf{n}_j = [\mathbf{n}_j^T (\lambda_{si}^b \times \mathbf{n}_j)^T] \begin{bmatrix} \dot{v}_i^b \\ \dot{\omega}_i^b \end{bmatrix} + [\omega_i^b \times (\omega_i^b \times \lambda_{si}^b)]^T \mathbf{n}_j \quad (10)$$

where  $j$  represents the direction of prismatic pair and  $j = (x,y,z)$ .

$$\begin{bmatrix} \dot{v}_i^b \\ \dot{\omega}_i^b \end{bmatrix} = \mathbf{J}_s \mathbf{A}_s + (\mathbf{V}_s)^T \mathbf{H}_r \mathbf{V}_s \quad (11)$$

where  $\mathbf{A}_s = [\ddot{z}_i^b, \ddot{\alpha}_i^b, \ddot{\beta}_i^b]^T$ .  $\mathbf{H}_r$  is a  $6 \times 3 \times 3$  Hessian matrix and  $\mathbf{H}_r = [\mathbf{h}_1 \mathbf{h}_2 \mathbf{h}_3 \mathbf{h}_4 \mathbf{h}_5 \mathbf{h}_6]^T$ .  $\mathbf{h}_3$  and  $\mathbf{h}_5$  are 3-order matrix whose element is zero.

$$\mathbf{h}_1 = \begin{bmatrix} 0 & 0 & 0 \\ 0 & \frac{\partial^2 x_i^b}{\partial \alpha_i^b \partial \alpha_i^b} & \frac{\partial^2 x_i^b}{\partial \beta \partial \alpha_i^b} \\ 0 & \frac{\partial^2 x_i^b}{\partial \alpha_i^b \partial \beta_i^b} & \frac{\partial^2 x_i^b}{\partial \beta_i^b \partial \beta_i^b} \end{bmatrix} \quad \mathbf{h}_2 = \begin{bmatrix} 0 & 0 & 0 \\ 0 & \frac{\partial^2 y_i^b}{\partial \alpha_i^b \partial \alpha_i^b} & 0 \\ 0 & 0 & 0 \end{bmatrix} \quad (12)$$

$$\mathbf{h}_4 = \begin{bmatrix} 0 & 0 & 0 \\ 0 & 0 & 0 \\ 0 & -\sin \beta_i^b & 0 \end{bmatrix} \quad \mathbf{h}_6 = \begin{bmatrix} 0 & 0 & 0 \\ 0 & 0 & 0 \\ 0 & -\cos \beta_i^b & 0 \end{bmatrix} \quad (13)$$

## 4. Dynamics analytical modeling of parallel mechanism with actuation redundancy

Based on kinematics analysis, Newton–Euler method is used to establish the dynamic model of parallel posture alignment mechanism. When establishing modeling, the friction force at the spherical hinge is neglected, and the influence of the friction force between the prismatic pair of the positioner is considered. The distributed force is simplified to a concentrated force.

### 4.1. Establishment of dynamic equation

During dynamic modeling, force analysis of each component is required. The force analysis of the moving platform is shown in Fig. 2.  ${}^i \mathbf{F}_i^p$  denotes the constraint force acting on the spherical hinge relative to the global coordinate system.  ${}^o \mathbf{F}_i^p$  and  ${}^o \mathbf{M}_i^p$  represent the equivalent external force and moment acting on the moving platform relative to the global coordinate system, respectively.  $m_i$  denotes the mass of the moving platform.  $g$  represents the gravity acceleration relative to the global coordinate system and  $\mathbf{g} = [0, 0, -9.8 \text{ m/s}^2]^T$ . When dynamic modeling is performed, kinematic chain and joint deformation are ignored.

Newton equation and Euler equation of moving platform are established relative to the global coordinate system.

$$\sum_{i=1}^4 {}^i \mathbf{F}_i^p + m_i \mathbf{g} + {}^o \mathbf{F}_i^b = m_i \mathbf{A}_s \quad (14)$$

$$\sum_{i=1}^4 (\mathbf{R}_i^b \lambda_{si}^t) \times {}^i \mathbf{F}_i^p + {}^o \mathbf{M}_i^b = \mathbf{I}_b \dot{\omega}_i^b + \omega_i^b \times (\mathbf{I}_b \omega_i^b)$$

where  $\mathbf{R}_i^b$  and  $\mathbf{I}_b$  represent the posture transform matrix and inertia matrix of the moving platform relative to global coordinate system [22], respectively.  $\mathbf{I}_i$  denotes inertia matrix of moving platform relative to moving platform coordinate system and  $\mathbf{I}_b = \mathbf{R}_i^b \mathbf{I}_i (\mathbf{R}_i^b)^T$ .

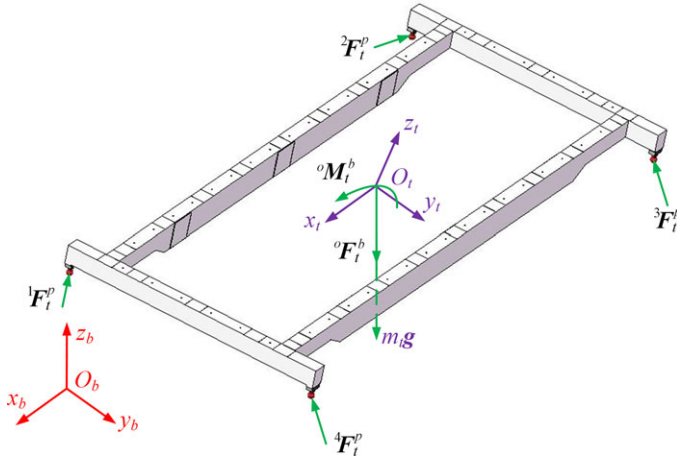


Figure 2. Force and moment analysis of moving platform.

The component analyzed in Figs. 3(a)–(d) is defined as component 3x, component 3y, component 3z and component 3r, respectively.  $l_{3z}^{Fu}$  and  $l_{3z}^{Fd}$  denote the arm of force and in Fig. 3(a), respectively.  $m_3^z$  denote the mass of components 3z. Newton equation and Euler equation of each analysis object of positioner are established in the global coordinate system. Take positioner 3 as an example to analyze the force of each component, as shown in Fig. 3. Coulomb friction and elastoplastic friction between different parts are considered. According to the mass and installation position of each part, the centroid position of each part of positioner can be calculated. The dynamic equations of each component of positioner 3 are established as follows.

See Fig. 3(a) for the stress analysis of telescopic rod of positioner 3 and define  $\mathbf{a}_3^z = [0, 0, a_3^z]^T$ . Then, the Newton–Euler equation of component 3z are written as:

$${}^e\mathbf{F}_{3x}^{3z} + {}^n\mathbf{F}_{3x}^{3z} + {}^d\mathbf{F}_3^z + m_3^z\mathbf{g} - {}^3\mathbf{F}_t^p = m_3^z\mathbf{a}_3^z \tag{15}$$

$$l_{3z}^{Fd}(-\mathbf{n}_3^z \times {}^n\mathbf{F}_{3x}^{3z}) + l_{3z}^{Fu}[\mathbf{n}_3^z \times (-{}^3\mathbf{F}_t^p)] + {}^s\mathbf{M}_{3x}^{3z} = \mathbf{E}_0 \tag{16}$$

where  $\mathbf{F}_{3x}^{3z}$  and  ${}^s\mathbf{M}_{3x}^{3z}$  represent the force and moment of component 3x applied on component 3z, respectively.  ${}^n\mathbf{F}_{3x}^{3z}$  and  ${}^e\mathbf{F}_{3x}^{3z}$  represent the perpendicular and parallel components of the spatial force to the z-axis, respectively.  ${}^d\mathbf{F}_3^z$  indicates the driving force acting on the telescopic rod, and the definitions of other driving force symbols are defined similarly.  $\mathbf{n}_3^z$  represents the direction vector of the z-direction prismatic pair of positioner 3, and the other direction vectors are defined similarly.  $\mathbf{E}_0 = [0, 0, 0]^T$ .

The force analysis of components 3x, 3y and 3r is shown in Figs. 3(b)–(d), whose Newton–Euler equation is given as:

$$m_3^x\mathbf{g} - {}^d\mathbf{F}_3^x - {}^e\mathbf{F}_{3x}^{3z} - {}^n\mathbf{F}_{3x}^{3z} + {}^e\mathbf{F}_{3y}^{3x} + {}^n\mathbf{F}_{3y}^{3x} = m_3^x\mathbf{a}_3^x \tag{17}$$

$$l_{3x}^{Fd}[\mathbf{n}_3^z \times ({}^e\mathbf{F}_{3y}^{3x} + {}^n\mathbf{F}_{3y}^{3x})] + l_{3x}^{Fu}[\mathbf{n}_3^z \times (-{}^n\mathbf{F}_{3x}^{3z})] - {}^s\mathbf{M}_{3x}^{3z} + {}^s\mathbf{M}_{3y}^{3x} = \mathbf{E}_0 \tag{18}$$

$${}^e\mathbf{F}_{3r}^{3y} + {}^n\mathbf{F}_{3r}^{3y} - {}^e\mathbf{F}_{3y}^{3x} - {}^n\mathbf{F}_{3y}^{3x} + m_3^y\mathbf{g} = m_3^y\mathbf{a}_3^y \tag{19}$$

$$(l_{3y}^{Fu}\mathbf{n}_3^z + d_3^x\mathbf{n}_3^x) \times (-{}^e\mathbf{F}_{3y}^{3x} - {}^n\mathbf{F}_{3y}^{3x}) + l_{3y}^{Fd}[-\mathbf{n}_3^z \times ({}^e\mathbf{F}_{3r}^{3y} + {}^n\mathbf{F}_{3r}^{3y})] + {}^s\mathbf{M}_{3r}^{3y} - {}^s\mathbf{M}_{3y}^{3x} = \mathbf{E}_0 \tag{20}$$

$$\mathbf{F}_{gd}^{3r} - {}^e\mathbf{F}_{3r}^{3y} - {}^n\mathbf{F}_{3r}^{3y} + m_3^r\mathbf{g} = \mathbf{E}_0 \tag{21}$$

$${}^s\mathbf{M}_{gd}^{3r} + l_{3r}^{Fd}(-\mathbf{n}_3^z \times \mathbf{F}_{gd}^{3r}) + (l_{3r}^{Fu}\mathbf{n}_3^z + d_3^y\mathbf{n}_3^y) \times (-{}^e\mathbf{F}_{3r}^{3y} - {}^n\mathbf{F}_{3r}^{3y}) - {}^s\mathbf{M}_{3r}^{3y} = \mathbf{E}_0 \tag{22}$$

where the variables in Eqs. (17)–(22) are similar to those in the previous equation.

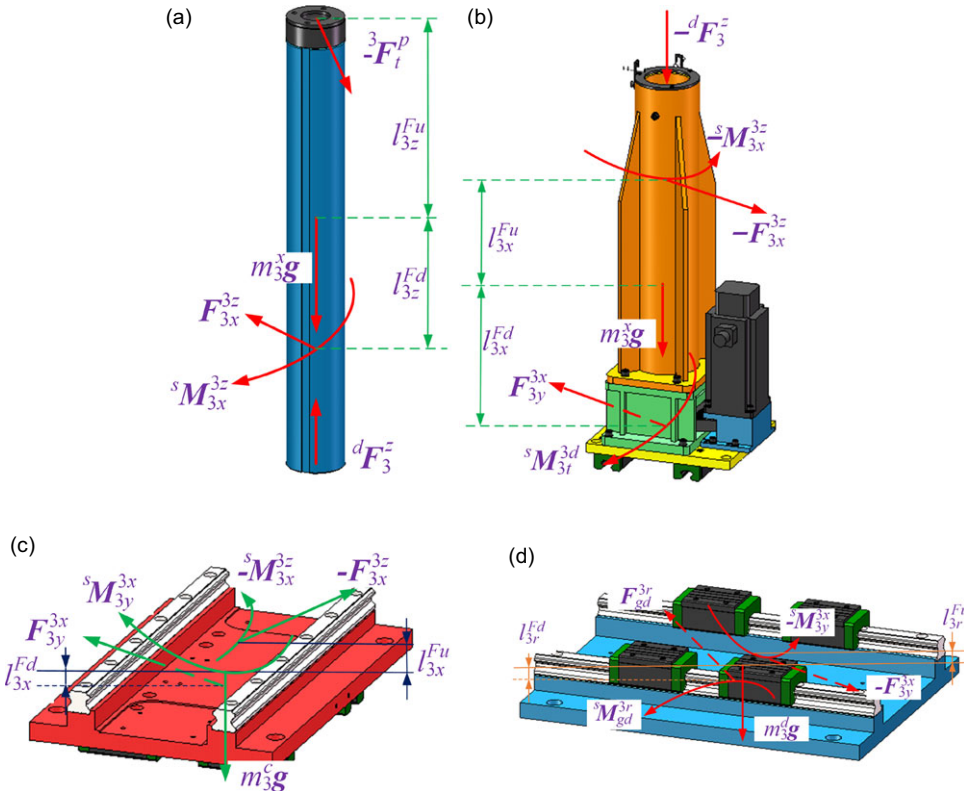


**Figure 3.** Force analysis diagram of positioner 3. (a) Force analysis of component 3z. (b) Force analysis of component 3y. (c) Force analysis of component 3z. (d) Force analysis of component 3r.

Elastoplastic friction model [23] considers the influence of elastic–plastic deformation of parts on friction, which is suitable for the calculation of friction when considering the elastic deformation of telescopic rod. On the premise that the friction calculation accuracy meets the requirements, to improve the efficiency of the algorithm, the Coulomb friction model is used to calculate the friction of telescopic rod. When the friction between prismatic pairs is taken into consideration, the friction is calculated as follows:

$${}^e\mathbf{F}_{3x}^{3z} = -\mu_c |{}^n\mathbf{F}_{3x}^{3z}| \operatorname{sgn}(v_3^z) \mathbf{n}_3^z \tag{23}$$

$${}^e\mathbf{F}_{3y}^{3x} = \sigma_0 z_3^x + \sigma_1 v_3^x \left( 1 - \frac{\sigma(z_3^x, v_3^x) z_3^x \sigma_0}{\mu_c (|{}^n\mathbf{F}_{3y}^{3x} \cdot \mathbf{n}_3^z| + |{}^n\mathbf{F}_{3y}^{3x} \cdot \mathbf{n}_3^y|) + [F_s - \mu_c (|{}^n\mathbf{F}_{3y}^{3x} \cdot \mathbf{n}_3^z| + |{}^n\mathbf{F}_{3y}^{3x} \cdot \mathbf{n}_3^y|)] e^{-\left(\frac{v_3^x}{v_s^x}\right)^{j_s}}} \right) + \sigma_2 v_3^x \tag{24}$$

$${}^e\mathbf{F}_{3r}^{3y} = \sigma_0 z_3^y + \sigma_1 v_3^y \left( 1 - \frac{\sigma(z_3^y, v_3^y) z_3^y \sigma_0}{\mu_c (|{}^n\mathbf{F}_{3r}^{3y} \cdot \mathbf{n}_3^z| + |{}^n\mathbf{F}_{3r}^{3y} \cdot \mathbf{n}_3^x|) + [F_s - \mu_c (|{}^n\mathbf{F}_{3r}^{3y} \cdot \mathbf{n}_3^z| + |{}^n\mathbf{F}_{3r}^{3y} \cdot \mathbf{n}_3^x|)] e^{-\left(\frac{v_3^y}{v_s^y}\right)^{j_s}}} \right) + \sigma_2 v_3^y \tag{25}$$



where  $\mu_c$  represents Coulomb friction coefficient and  $\text{sgn}$  represents step function.  $F_s$  denotes static friction force.  $\sigma_0$  represents the stiffness coefficient.  $z_3^x$  and  $z_3^y$  stand for average deflection of the contacting asperities,  $\sigma_1$  denotes the damping coefficient of the bristle,  $\sigma_2$  is the viscous friction coefficient.  $\sigma(z_3^x, v_3^x)$  and  $\sigma(z_3^y, v_3^y)$  stand for the zones of the elastic and plastic deformation of asperities.  $v_s$  represents the Stribeck velocity.  $j_s$  denotes the Stribeck shape factor.

Newton equations and Euler equations of the other positioners can be established using similar methods. Since the number of unknowns 95 is more than the number of equations 93, there are multiple sets of solutions to the driving force, so it is difficult to accurately calculate. Therefore, it is necessary to supplement the constraint equations.

4.1.1. Mapping relationship between position uncertainty of follow-up prismatic pair and pose error of moving platform

For parallel mechanism with actuation redundancy, there are many ways to increase the number of constraint equations, for example, minimizing the position errors [10] and internal force regulation [24]. Based on the deformation compatibility equation, the paper increases the number of constraint equations. Taking the third branch chain as an example, the establishment process of the mapping relationship between the telescopic rod deformation and the pose error of the moving platform is introduced in detail.

The telescopic rod is regarded as a cantilever beam. Under the action of spatial force, the position error of  $S_i$  relative to  $O_i, \delta\lambda_{si}^t$  can be expressed as [25]:

$$\delta\lambda_{si}^t = \begin{bmatrix} \frac{-i F_t^p L_{ii}^3}{3EI} & \frac{-i F_t^p L_{ii}^3}{3EI} & \frac{-i F_t^p L_{iz}}{EA} \end{bmatrix}^T \tag{26}$$

where  $L_{ii}$  denotes the length of component  $iz$  extending from component  $ix$ .  $L_{iz}$  stands for the length of component  $iz$ .  $A, E$  and  $I$  represent the cross-section area, elastic modulus and polar moment of inertia of component  $iz$ , respectively.

$\mathbf{n}_i^x, \mathbf{n}_i^y$  and  $\mathbf{n}_i^z$  represent the direction vectors of each prismatic pair, respectively.  $\lambda_{oi}^b$  denotes the origin of positioner  $i$  coordinate system in the global coordinate system.  $d_i^x, d_i^y$  and  $d_i^z$  denote the displacement of each prismatic pair of the positioner. Eq. (27) can be obtained by the space vector chain method:

$$\lambda_{oi}^b + d_i^x \mathbf{n}_i^x + d_i^y \mathbf{n}_i^y + d_i^z \mathbf{n}_i^z = \mathbf{P}_i^b + \mathbf{R}_i^b \lambda_{si}^t \tag{27}$$

Considering the axial deformation and bending deformation of the telescopic rod under the action of external force and torque, Eq. (28) is established as follows:

$$\lambda_{oi}^b + (d_i^x + \delta d_i^x) \mathbf{n}_i^x + (d_i^y + \delta d_i^y) \mathbf{n}_i^y + d_i^z \mathbf{n}_i^z + \delta S_i = \mathbf{P}_i^b + \delta \mathbf{P}_i^b + (\delta \mathbf{R}_i^b + \mathbf{R}_i^b) \lambda_{si}^t \tag{28}$$

where the elastic deformation of moving platform,  $x$  and  $y$  prismatic pair is ignored, so there is no parameter term related to  $\delta \mathbf{n}_i^x, \delta \mathbf{n}_i^y, \delta \mathbf{n}_i^z, \delta \lambda_{si}^t$  and  $\delta \lambda_{oi}^b$ .  $z$ -direction prismatic pair is driven by servo motor and ball screw, so the position error is very small and can be ignored.  $\delta S_i$  denotes the spatial variation of point  $S_i$  caused by the deformation of the telescopic rod, and  $\delta S_i = [\delta S_i^x, \delta S_i^y, \delta S_i^z]^T$ .  $\delta d_i^x$  and  $\delta d_i^y$  represent the positional errors of the follow-up prismatic pair of positioner  $i$  in the  $x$  direction and  $y$  direction, respectively.  $\delta \mathbf{P}_i^b$  and  $\delta \mathbf{R}_i^b$  represent the position error and the differential of rotation matrix of moving platform [26], respectively.

$$\delta \mathbf{P}_i^b = \begin{bmatrix} \delta x_i^b & \delta y_i^b & \delta z_i^b \end{bmatrix}^T \tag{29}$$

$$\delta \mathbf{R}_i^b = \begin{bmatrix} 0 & -\delta \gamma_i^b & \delta \beta_i^b \\ \delta \gamma_i^b & 0 & -\delta \alpha_i^b \\ -\delta \beta_i^b & \delta \alpha_i^b & 0 \end{bmatrix} \mathbf{R}_i^b = \Omega_{3 \times 3} \mathbf{R}_i^b \tag{30}$$

where  $\delta x_t^b, \delta y_t^b, \delta z_t^b, \delta \alpha_t^b, \delta \beta_t^b$  and  $\delta \gamma_t^b$  represent pose error of moving platform. It can be obtained from Eq. (28) that:

$$\lambda_{oi}^b + d_i^x \mathbf{n}_i^x + \delta d_i^x \mathbf{n}_i^x + d_i^y \mathbf{n}_i^y + \delta d_i^y \mathbf{n}_i^y + d_i^z \mathbf{n}_i^z + \delta d_i^z \mathbf{n}_i^z + \delta \mathbf{S}_i = \mathbf{P}_t^b + \delta \mathbf{P}_t^b + \delta \mathbf{R}_t^b \lambda_{si}^t + \mathbf{R}_t^b \lambda_{si}^t \tag{31}$$

Eq. (32) can be built by subtracting Eq. (27) from Eq. (31):

$$\delta d_i^x \mathbf{n}_i^x + \delta d_i^y \mathbf{n}_i^y + \delta \mathbf{S}_i = \delta \mathbf{P}_t^b + \delta \mathbf{R}_t^b \lambda_{si}^t \tag{32}$$

Eq. (33) is established by matrix vector multiplication:

$$\delta d_i^x + \delta \mathbf{S}_i \cdot \mathbf{n}_i^x = (\delta \mathbf{P}_t^b + \delta \mathbf{R}_t^b \lambda_{si}^t) \cdot \mathbf{n}_i^x = (\delta \mathbf{P}_t^b + \Omega_{3 \times 3} \mathbf{R}_t^b \lambda_{si}^t) \cdot \mathbf{n}_i^x \tag{33}$$

There is the following definition,

$$\mathbf{R}_t^b \lambda_{si}^t = \zeta_i \tag{34}$$

where  $\zeta_i = [\zeta_i^x, \zeta_i^y, \zeta_i^z]^T$ , which is a known quantity. Then, Eq. (32) can be sorted as:

$$\delta d_i^x + \delta \mathbf{S}_i \cdot \mathbf{n}_i^x = \delta d_i^x + \delta \mathbf{S}_i^T \mathbf{n}_i^x = (\delta \mathbf{P}_t^b + \Omega_{3 \times 3} \zeta_i) \cdot \mathbf{n}_i^x = \mathbf{Q}_i \delta \mathbf{M} \tag{35}$$

where

$$\mathbf{Q}_i = [1 \quad 0 \quad 0 \quad 0 \quad \zeta_i^z \quad -\zeta_i^y] \tag{36}$$

$$\delta \mathbf{M} = [\delta x_t^b \quad \delta y_t^b \quad \delta z_t^b \quad \delta \alpha_t^b \quad \delta \beta_t^b \quad \delta \gamma_t^b]^T \tag{37}$$

Evidenced by the same token,

$$\delta d_i^y + \delta \mathbf{S}_i \cdot \mathbf{n}_i^y = \delta d_i^y + \delta \mathbf{S}_i^T \mathbf{n}_i^y = [0 \quad 1 \quad 0 \quad -\zeta_i^z \quad 0 \quad \zeta_i^x] \delta \mathbf{M} \tag{38}$$

$$\delta \mathbf{S}_i^T \mathbf{n}_i^z = [0 \quad 0 \quad 1 \quad \zeta_i^y \quad -\zeta_i^x \quad 0] \delta \mathbf{M} \tag{39}$$

Eq. (40) can be obtained by further analysis,

$$\Delta \mathbf{d} + \Delta \mathbf{S} \mathbf{N} = \mathbf{Q} \delta \mathbf{M} \tag{40}$$

where

$$\Delta \mathbf{d} = [0 \quad \dots \quad \delta d_3^x \quad \dots \quad \delta d_4^y \quad 0]^T_{12 \times 1} \tag{41}$$

$$\mathbf{N} = [(\mathbf{n}_1^x)^T \quad (\mathbf{n}_1^y)^T \quad \dots \quad (\mathbf{n}_4^z)^T]^T_{36 \times 1} \tag{42}$$

$$\Delta \mathbf{S} = \begin{bmatrix} \delta \mathbf{S}_1^T & \mathbf{E}_0^T & \dots & \mathbf{E}_0^T & \mathbf{E}_0^T \\ \mathbf{E}_0^T & \delta \mathbf{S}_1^T & \dots & \mathbf{E}_0^T & \mathbf{E}_0^T \\ \vdots & \vdots & \ddots & \vdots & \vdots \\ \mathbf{E}_0^T & \mathbf{E}_0^T & \dots & \mathbf{E}_0^T & \delta \mathbf{S}_4^T \end{bmatrix}_{12 \times 36} \tag{43}$$

$$\mathbf{Q} = \begin{bmatrix} 1 & 0 & 0 & 0 & \zeta_1^z & -\zeta_1^y \\ 0 & 1 & 0 & -\zeta_1^z & 0 & \zeta_1^x \\ \vdots & \vdots & \vdots & \vdots & \vdots & \vdots \\ 0 & 0 & 1 & \zeta_4^y & -\zeta_4^z & 0 \end{bmatrix}_{12 \times 6} \tag{44}$$

Positioner 1 does not install prismatic pair in  $x$  and  $y$  direction, and positioner 2 has no prismatic pair in  $y$  direction. The positional error of prismatic pairs in  $z$  direction is extremely small, and the corresponding positional error is 0. So far, the mapping relationship between the deformation of the telescopic rod and the pose error of the moving platform can be established.

4.1.2. Deformation supplementary equation based on flexibility analysis

Under the internal force of the parallel posture alignment system, the elastic deformation matrix of the telescopic rod can be expressed as:

$$\Delta \mathbf{S}_{12 \times 36} = \mathbf{F}_{12 \times 36} \mathbf{C}_{36 \times 36} \tag{45}$$

where  $\mathbf{C}$  represents the flexibility matrix of the telescopic rod.

$$\mathbf{F} = \begin{bmatrix} {}^1F_t^x & {}^1F_t^y & {}^1F_t^z & 0 & \dots & 0 & 0 \\ 0 & 0 & 0 & {}^1F_t^x & \dots & 0 & 0 \\ \vdots & \vdots & \vdots & \vdots & \ddots & \vdots & \vdots \\ 0 & 0 & 0 & 0 & \dots & 0 & 0 \\ 0 & 0 & 0 & 0 & \dots & {}^4F_t^y & {}^4F_t^z \end{bmatrix} \tag{46}$$

where  $({}^1F_t^x, {}^1F_t^y, {}^1F_t^z)^T = {}^1F_t^p$

$$\mathbf{C} = \begin{bmatrix} \frac{-L_{11}^3}{EI} & 0 & 0 & \dots & 0 & 0 \\ 0 & \frac{-L_{11}^3}{EI} & 0 & \dots & 0 & 0 \\ \vdots & \vdots & \vdots & \ddots & \vdots & \vdots \\ 0 & 0 & 0 & \dots & \frac{-L_{44}^3}{EI} & 0 \\ 0 & 0 & 0 & \dots & 0 & \frac{-L_{4z}}{EA} \end{bmatrix} \tag{47}$$

As shown in Fig. 4(a), the follow-up prismatic pair moves under the internal force of the parallel posture alignment system and affected by the friction force of the prismatic pair. The deformation of the telescopic rod is related to the friction. The force component at the spherical hinge is similar to the friction when adjust the parallel posture alignment system with low accelerations. Therefore, the force component at the spherical hinge is used to replace the friction to calculate the deformation of telescopic rod. Then, the deformation at the top of the telescopic rod is equivalent to the position uncertainty of the follow-up prismatic pair, as shown in Fig. 4(b). In Fig. 4, the solid line represents the actual situation and the dotted line represents the ideal situation.

The dynamic supplementary equation can be obtained by simultaneous Eqs. (40) and (45),

$$\Delta \mathbf{d}_{12 \times 1} + \mathbf{F}_{12 \times 36} \mathbf{C}_{36 \times 36} \mathbf{N}_{36 \times 1} = \mathbf{Q}_{12 \times 6} \delta \mathbf{M}_{6 \times 1} \tag{48}$$

Through deformation coordination analysis, Eq. (48) establishes the correlation equation among  $\delta \mathbf{R}_t^b$  and  $\delta \mathbf{P}_t^b, d_t^x, d_t^y$  and  $d_t^z$ . 12 linearly independent constraint equations are supplemented. The spatial position of the spherical hinge in the moving platform coordinate system remains unchanged, so Eqs. (49) and (50) are established.

$$\delta \mathbf{S}_1 + \delta \mathbf{S}_3 = \delta \mathbf{S}_2 + \delta \mathbf{S}_4 \tag{49}$$

$$(\lambda_{s1}^t - \lambda_{s2}^t + \delta \mathbf{S}_1 - \delta \mathbf{S}_2) \cdot (\lambda_{s3}^t - \lambda_{s2}^t + \delta \mathbf{S}_3 - \delta \mathbf{S}_2) = 0 \tag{50}$$

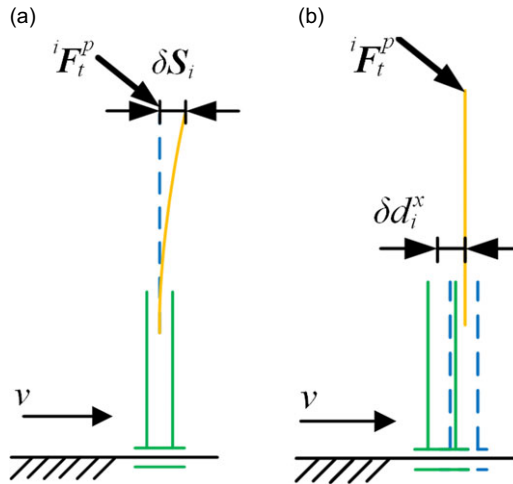


**Figure 4.** Structural deformation and positional error. (a) Deformation of telescopic rod. (b) Position uncertainty of follow-up prismatic pair.

There are three constraint equations in Eq. (49) and one constraint equation in Eq. (50). Higher-order terms such as  $\delta S_1 \delta S_2$ ,  $\delta S_2 \delta S_3$  and  $\delta S_2^2$  are ignored in Eq. (50). So Eq. (50) can be simplified as a first-order equation related to  $\delta S_1$ ,  $\delta S_2$  and  $\delta S_3$ . Eqs. (14)–(25) and Eqs. (48)–(50) contain 124 constraint equations and 124 unknowns. Therefore, the driving force can be solved.

#### 4.2. Solution of force acting on spherical hinge

Maple [27] or Mathematics [28] can be used to solve the equations, but the equations cannot be solved in a short time. The least square method [29] and other numerical methods can be used to solve the unknown variables in the dynamic equation, which does not require complex analytical modeling. However, the accuracy of the solution is greatly affected by the initial iteration values, so it is difficult to obtain exact solutions. The unknowns in the dynamic equation can be solved by analytic analysis, that is, the mathematical expression of the unknowns can be obtained. In the analytical modeling, the driving force at the spherical hinge is first solved by taking the moving platform as the analytical object, then the force at the spherical hinge is brought into the dynamic equation of each branch and the analytical solution of the branch equation is solved.

It can be seen from Eq. (5) that the displacement of prismatic pair is only related to  $z_i^b$ ,  $\alpha_i^b$  and  $\beta_i^b$ . Therefore, the motion trajectory of the posture alignment mechanism is only related to  $z_i^b$ ,  $\alpha_i^b$  and  $\beta_i^b$ . Assuming that the trajectory of the parallel posture alignment mechanism is known, that is,  $z_i^b$ ,  $\alpha_i^b$  and  $\beta_i^b$  are known quantities. In Eqs. (14), (48), (49) and (50), the unknown is the force at the spherical hinge and the position uncertainty of the follow-up prismatic pair. The unknown number is 22 and the number of equations is 22.

In Eq. (14), only  $A_f$  is the first-order function of  ${}^1 F_t^p$ ,  ${}^2 F_t^p$ ,  ${}^3 F_t^p$  and  ${}^4 F_t^p$  are unknowns. In Eq. (48), only the parameters are unknown. After sorting out Eqs. (14), (48), (49) and Eqs. (50), (51) can be obtained:

$$A_f X_f = B_f \tag{51}$$

where  $A_f$  is the first-order function of  ${}^1 F_t^p$ ,  ${}^2 F_t^p$ ,  ${}^3 F_t^p$  and  ${}^4 F_t^p$ .  $B_f$  is the function of  $m_t \ddot{q}$ ,  $m_{dr} g$ ,  ${}^o F_t^b$ ,  $I_b \dot{\omega}_t^b$ ,  $\omega_t^b \times (I_b \omega_t^b)$  and  ${}^o M_t^b$ .  $A_f$  is a matrix of order 22, whose expression is known. Therefore, the force at each spherical joint can be solved,

$$X_f = (A_f)^{-1} B_f \tag{52}$$

**4.3. Solution of driving force based on vector mixed product**

After calculating the force at the spherical joint, take the force at the spherical joint as the intermediate variable to calculate the driving force required by each active prismatic pair. Taking the force at the spherical hinge as the intermediate variable, the driving force of the branch chain can be solved. According to the principle of mixed product of vector, multiply Eq. (15) by vector  $\mathbf{n}_3^z$  and then multiply by  $l_{3z}^{Fd}$ , Eq. (53) can be obtained:

$$l_{3z}^{Fd}(\mathbf{n}_3^z \times {}^n\mathbf{F}_{3x}^{3z}) + l_{3z}^{Fd}(\mathbf{n}_3^z \times {}^d\mathbf{F}_3^c) - l_{3z}^{Fd}(\mathbf{n}_3^z \times {}^3\mathbf{F}_t^p) = \mathbf{E}_0 \tag{53}$$

After adding Eqs. (53) to (16), Eq. (54) can be obtained:

$${}^s\mathbf{M}_{3x}^{3z} = (l_{3z}^{Fd} + l_{3z}^{Fu}) (\mathbf{n}_3^z \times {}^3\mathbf{F}_t^p) \tag{54}$$

Based on Eqs. (16), (55) can be obtained by multiplying the left cross of the vector  $\mathbf{n}_3^z$  and expanding it according to the triple product of the vector:

$${}^n\mathbf{F}_{3x}^{3z} = \frac{1}{l_{3z}^{Fd}} \{ l_{3z}^{Fu} [\mathbf{n}_3^z (\mathbf{n}_3^z \cdot {}^3\mathbf{F}_t^p) - {}^3\mathbf{F}_t^p] - \mathbf{n}_3^z \times {}^s\mathbf{M}_{3x}^{3z} \} \tag{55}$$

Substituting Eq. (54) into Eq. (55) gives:

$${}^n\mathbf{F}_{3x}^{3z} = {}^3\mathbf{F}_t^p - \mathbf{n}_3^z (\mathbf{n}_3^z \cdot {}^3\mathbf{F}_t^p) \tag{56}$$

Additionally, substituting Eq. (56) into Eq. (23) gives:

$${}^e\mathbf{F}_{3x}^{3z} = -\mu_c |{}^3\mathbf{F}_t^p - \mathbf{n}_3^z (\mathbf{n}_3^z \cdot {}^3\mathbf{F}_t^p)| \operatorname{sgn}(v_3^z) \mathbf{n}_3^z \tag{57}$$

According to Eq. (15),  ${}^d\mathbf{F}_3^c$  can be expressed as:

$${}^d\mathbf{F}_3^c = m_3^z \mathbf{a}_3^z + {}^3\mathbf{F}_t^p - m_3^z \mathbf{g} - {}^e\mathbf{F}_{3x}^{3z} - {}^n\mathbf{F}_{3x}^{3z} \tag{58}$$

Substituting Eqs. (57) and (56) into Eq. (58) gives:

$${}^d\mathbf{F}_3^c = m_3^z \mathbf{a}_3^z - m_3^z \mathbf{g} - \mu_c |{}^3\mathbf{F}_t^p - \mathbf{n}_3^z (\mathbf{n}_3^z \cdot {}^3\mathbf{F}_t^p)| \operatorname{sgn}(v_3^z) \mathbf{n}_3^z + \mathbf{n}_3^z (\mathbf{n}_3^z \cdot {}^3\mathbf{F}_t^p) \tag{59}$$

Based on Eqs. (17), (60) can be obtained by multiplying the left cross of the vector  $\mathbf{n}_3^x$  twice and expanding it according to the triple product of the vector:

$${}^n\mathbf{F}_{3y}^{3x} = -m_3^x \mathbf{g} + {}^d\mathbf{F}_3^c + {}^e\mathbf{F}_{3x}^{3z} - \mathbf{n}_3^x (\mathbf{n}_3^x \cdot {}^n\mathbf{F}_{3x}^{3z}) + {}^n\mathbf{F}_{3x}^{3z} \tag{60}$$

Substituting Eqs. (57), (56) and (58) into Eq. (60) gives:

$${}^n\mathbf{F}_{3y}^{3x} = m_3^z \mathbf{a}_3^z - (m_3^z + m_3^x) \mathbf{g} + {}^3\mathbf{F}_t^p - \mathbf{n}_3^x (\mathbf{n}_3^x \cdot {}^3\mathbf{F}_t^p) \tag{61}$$

It can be seen from Eq. (17) that:

$$\mathbf{a}_3^x = (m_3^x \mathbf{g} - {}^d\mathbf{F}_3^c - {}^e\mathbf{F}_{3x}^{3z} - {}^n\mathbf{F}_{3x}^{3z} + {}^e\mathbf{F}_{3y}^{3x} + {}^n\mathbf{F}_{3y}^{3x}) / m_3^x \tag{62}$$

Substituting Eqs. (57) to (61) into Eq. (62) gives:

$$\mathbf{a}_3^x = \langle -\mathbf{n}_3^x (\mathbf{n}_3^x \cdot {}^3\mathbf{F}_t^p) - \mu_c \{ m_3^z \mathbf{a}_3^z - (m_3^z + m_3^x) \mathbf{g} + {}^3\mathbf{F}_t^p \} + |\mathbf{n}_3^y \cdot {}^3\mathbf{F}_t^p| \operatorname{sgn}(v_3^z) \mathbf{n}_3^z \rangle / m_3^x \tag{63}$$

Add Eqs. (15), (17) and (19), and Eq. (64) can be obtained:

$$m_3^z \mathbf{g} - {}^3\mathbf{F}_t^p + m_3^x \mathbf{g} + {}^e\mathbf{F}_{3r}^{3y} + {}^n\mathbf{F}_{3r}^{3y} + m_3^y \mathbf{g} = m_3^x \mathbf{a}_3^x + m_3^y \mathbf{a}_3^y + m_3^z \mathbf{a}_3^z \tag{64}$$

Based on Eqs. (64), (65) can be obtained by multiplying the left cross of the vector  $\mathbf{n}_3^y$  twice and expanding it according to the triple product of the vector:

$${}^n\mathbf{F}_{3r}^{3y} = m_3^z \mathbf{a}_3^z + m_3^x \mathbf{a}_3^x - (m_3^z + m_3^x + m_3^y) \mathbf{g} - \mathbf{n}_3^y (\mathbf{n}_3^y \cdot {}^3\mathbf{F}_t^p) + {}^3\mathbf{F}_t^p \tag{65}$$

${}^e\mathbf{F}_{3r}^{3y}$  and  ${}^e\mathbf{F}_{3y}^{3x}$  can be calculated by Eqs. (24), (25), (61) and (65).

**Table I.** Value of simulation parameters.

Symbol	Value
$m_1^z, m_2^z, m_3^z, m_4^z$	33.3 kg
$m_1^r$	70.8 kg
$m_3^r, m_4^r$	33.2 kg
$m_2^x, m_3^x, m_4^x$	75.9 kg
$m_3^y, m_4^y$	35.2 kg
$m_2^y$	30.0 kg
$l_{1z}^{Fd}, l_{2z}^{Fd}, l_{3z}^{Fd}, l_{4z}^{Fd}$	308 mm
$l_{2r}^{Fd}, l_{3r}^{Fd}, l_{4r}^{Fd}$	18.9 mm
$l_{3y}^{Fu}, l_{4y}^{Fu}, l_{2r}^{Fu}, l_{3r}^{Fu}, l_{4r}^{Fu}$	47.3 mm
$l_{1z}^{Fu}, l_{2z}^{Fu}, l_{3z}^{Fu}, l_{4z}^{Fu}$	382.5 mm
$l_{3y}^{Fd}, l_{4r}^{Fu}$	34.1 mm

The similar method can be used to calculate the driving force required by the remaining prismatic pair of positioners under the specified trajectory.

$${}^d\mathbf{F}_1^z = m_1^z \mathbf{a}_1^z - m_1^z \mathbf{g} + ({}^1\mathbf{F}_t^p \cdot \mathbf{n}_1^z) \mathbf{n}_1^z + \mu_c |{}^1\mathbf{F}_t^p - \mathbf{n}_1^z (\mathbf{n}_1^z \cdot {}^1\mathbf{F}_t^p)| \text{sgn}(v_1^z) \mathbf{n}_1^z \tag{66}$$

$${}^d\mathbf{F}_2^z = m_2^z \mathbf{a}_2^z - m_2^z \mathbf{g} + ({}^2\mathbf{F}_t^p \cdot \mathbf{n}_2^z) \mathbf{n}_2^z + \mu_c |{}^2\mathbf{F}_t^p - \mathbf{n}_2^z (\mathbf{n}_2^z \cdot {}^2\mathbf{F}_t^p)| \text{sgn}(v_2^z) \mathbf{n}_2^z \tag{67}$$

$${}^d\mathbf{F}_2^x = m_2^x \mathbf{a}_2^x + ({}^2\mathbf{F}_t^p \cdot \mathbf{n}_2^x) \mathbf{n}_2^x + \mu_c \{ |m_3^z \mathbf{a}_3^z - (m_3^z + m_3^x) \mathbf{g} + {}^3\mathbf{F}_t^p| + |\mathbf{n}_3^y \cdot {}^3\mathbf{F}_t^p| \} \text{sgn}(v_3^z) \mathbf{n}_3^z \tag{68}$$

The expressions for  ${}^d\mathbf{F}_4^z$  and  ${}^d\mathbf{F}_3^z$  are similar. Thus, the inverse dynamics modeling of the parallel posture alignment system with actuation redundancy can be realized. To analysis efficiency and verify the validity and applicability of the dynamics model, simulation analysis and experimental verification are carried out.

### 5. Simulation analysis

To prove the efficiency of the algorithm, the simulation analysis of analytical modeling method proposed is carried out. The simulation analysis is mainly used to compare the driving force solution time of the proposed algorithm and other methods and calculate the difference between the proposed algorithm and ADAMS software simulation.

To demonstrate the validity and applicability of the proposed method, trajectories should be defined to include moving and turning. The independent variables in the pose parameters are  $z_i^b$ ,  $\alpha_i^b$  and  $\beta_i^b$ .  $z_i^b$  makes the parallel posture alignment mechanism moving along the global coordinate system,  $\alpha_i^b$  and  $\beta_i^b$  make the parallel posture alignment mechanism turning around the global coordinate system axis. Therefore, the kinematic trajectory of the parallel posture alignment mechanism is defined as follows:

$$\begin{cases} z_i^b = 60 \sin(t) + 1240 \\ \alpha_i^b = t/300 \\ \beta_i^b = t/600 \end{cases} \tag{69}$$

where the unit of  $\alpha_i^b$  and  $\beta_i^b$  is radian. The unit of  $z_i^b$  is mm, and  $t$  represent simulation time whose unit is second.  $A = 5.5 \times 103 \text{ mm}^2$ ,  $I = 4.0 \times 106 \text{ mm}^4$ ,  $E = 2.05 \times 105 \text{ N/mm}^2$ ,  $l = 4410 \text{ mm}$ ,  $w = 2050 \text{ mm}$ ,  $h = 240 \text{ mm}$ ,  $m_t = 561 \text{ kg}$ . The remaining parameters are shown in Table I.

**Table II.** Comparison of calculation time of driving force.

Calculation method	Calculation time
The method proposed	13.85 ms
Moore Penrose contrastive analysis	31.68 ms

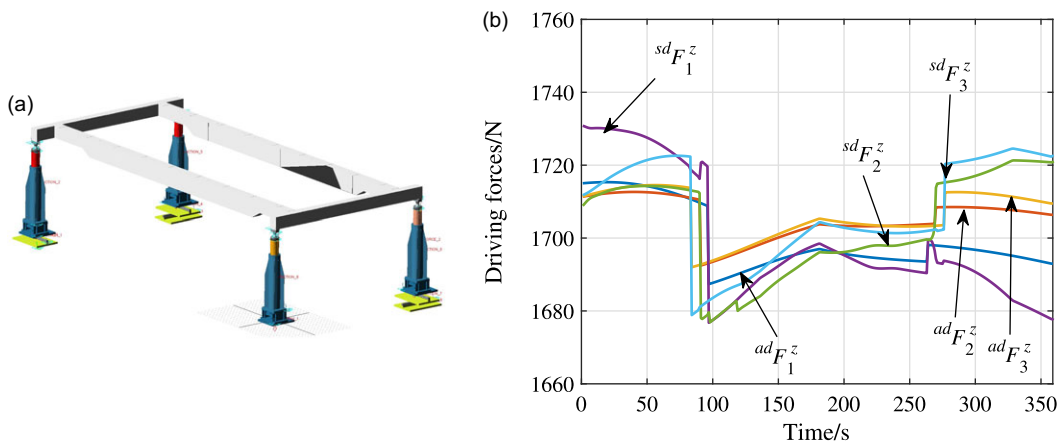


**Figure 5.** Driving force simulation. (a) Simulation model. (b) Simulation result.

**5.1. Analysis of algorithm efficiency**

To compare the running time of this algorithm with the existing algorithms, the driving force calculation time is analyzed, as shown in Table II. The computer configuration used for the inverse dynamics modeling is Intel Core i7-9750H CPU 2.60 GHz with 16G RAM.

It can be seen from Table II that the dynamic modeling method proposed has a shorter calculation time and high efficiency, which is 56.28% lower than Moore–Penrose [30] and has more advantages in the design of dynamic controllers. The dynamic modeling method proposed can improve the anti-interference and anti-noise performance of the parallel posture alignment mechanism.

**5.2. Analysis of validity and applicability**

To demonstrate the validity and applicability of the proposed method, ADAMS software is used to calculate the difference between the algorithm proposed in this paper and the simulation value, as shown in Fig. 5(a).

where  $ad F_1^z$ ,  $ad F_2^z$  and  $ad F_3^z$  represent the driving force calculated by the proposed method.  $sd F_1^z$ ,  $sd F_2^z$  and  $sd F_3^z$  denote the driving force calculated by ADAMS.

It can be seen from Fig. 5(b) that the maximum difference between the analytical modeling method proposed in this paper and ADAMS simulation results is 16.35N, and the maximum percentage of error is 0.97% which demonstrates the validity and applicability of the proposed method.

**6. Experiment verification**

To verify the validity and applicability of the proposed analytical method of driving force, an experimental study is carried out. The parameters of the mechanism are identified using the method in literature [23, 31] and computer-aided design. RS-485 [32] converter is used to read the drive current, as shown in Fig. 6.

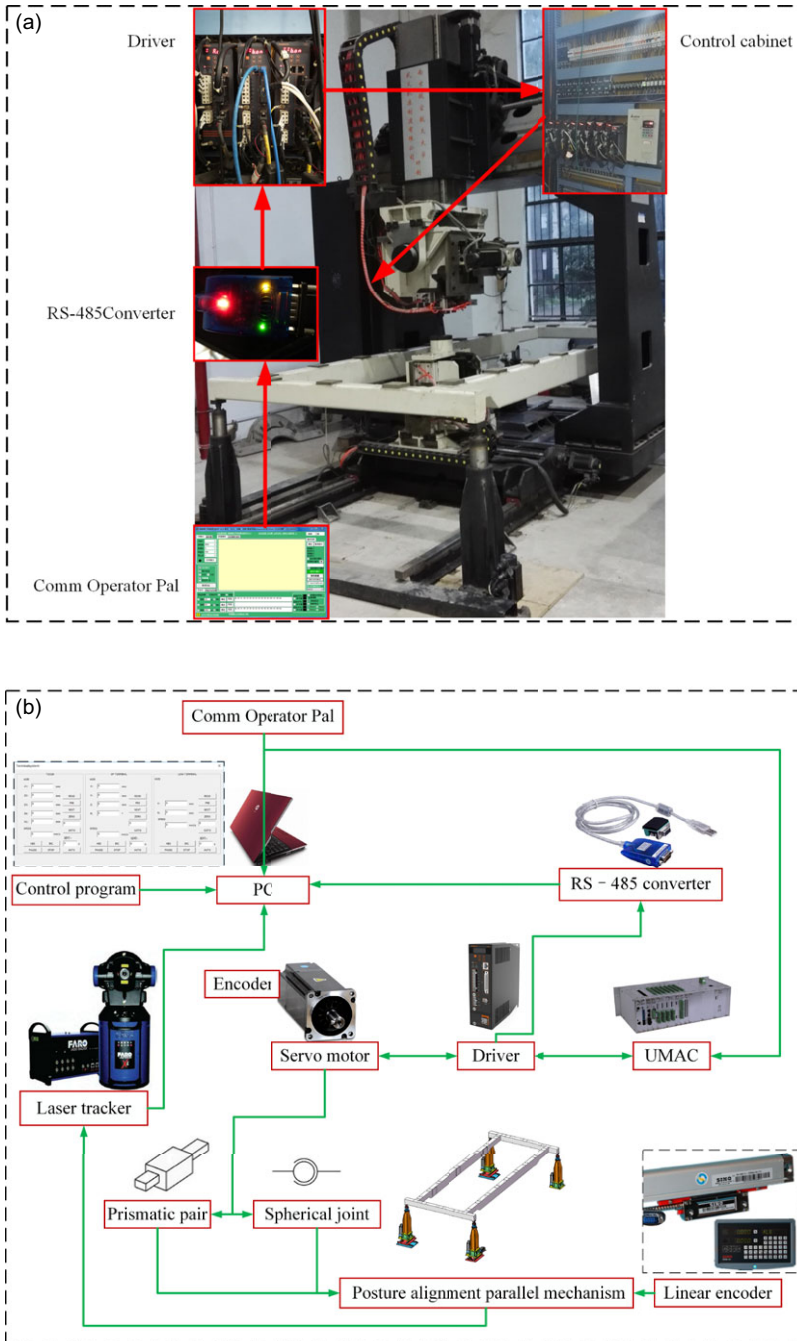


**Figure 6.** Read current information of driver. (a) The posture alignment parallel mechanism. (b) Driving force information transmission.

As shown in Fig. 6(a), a servo motor driver is installed in the control cabinet. The Comm Operator Pal can be installed on the computer, and the driver current information in the servo motor driver can be read through the RS-485 converter. The read and converted values are processed through the longitudinal redundancy check combined with the MATLAB wavelet denoising toolbox. As can be seen from Fig. 6(b), the kinematic pair of the parallel posture alignment mechanism includes prismatic pair and



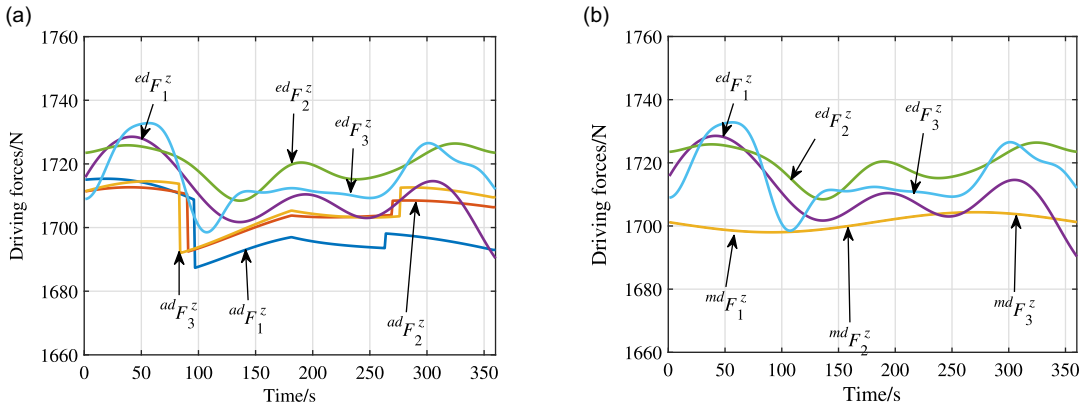


**Figure 7.** Driving force during experiment. (a) Precision analysis of the algorithm proposed in this paper. (b) Precision analysis of algorithms in existing literature.

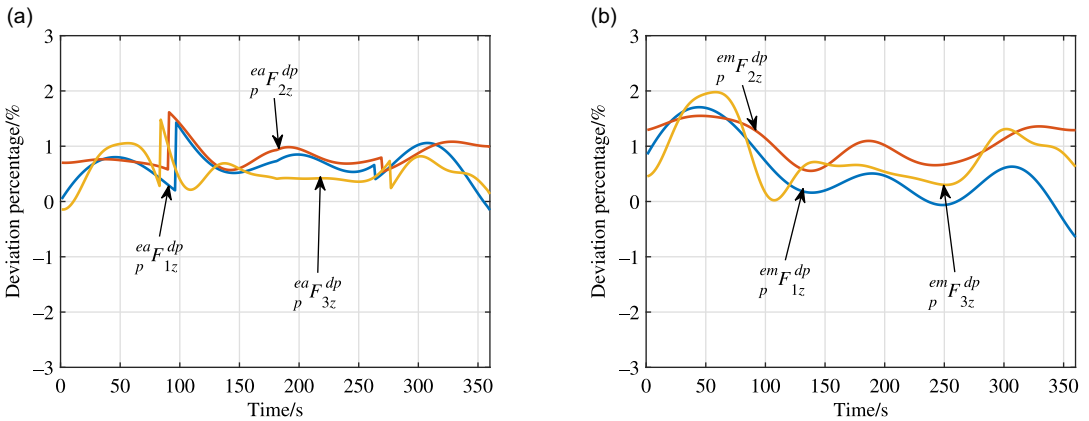


**Figure 8.** Deviation percentage comparison. (a) The deviation percentage of the algorithm proposed in this paper. (b) Comparative experiment of deviation percentage.

spherical joint pair. The control program in PC sends instructions to the driver through universal motion and automation controller, and the driver controls the motion of the servo motor. Using the laser tracker and the kinematics calibration algorithm, the structural parameters of the parallel posture alignment mechanism can be identified to increase the motion accuracy.

The  $z$ -direction prismatic pair of positioner 1, 2 and 3 adopts the position control mode [33]. The  $x$ -direction prismatic pair of positioner 2 and the  $z$ -direction prismatic pair of positioner 4 adopt the force control mode [34, 35]. The driving force of  $z$ -direction prismatic pair of positioner 1, 2 and 3 is analyzed to verify the effectiveness of the proposed modeling method.

The driver adopts absolute value encoder: speed response 1 KHz, circuit time parameter  $47 \mu s$ , maximum input pulse frequency 500K pps. Parameters of current sensor: accuracy 0.5%, linearity 0.2%, response time  $< 10 \mu s$ , bandwidth DC 100 kHz, temperature drift  $\leq 500 PPM/^\circ C$ . The driving force data is read every 0.1 s.

The current signal of servo motor driver is collected, and the drive current is translated into the driving force of prismatic pair. Wavelet denoising and curve fitting in MATLAB are used to process the collected information, and the corresponding driving force information is shown in Figs. 7 and 8.  $ed F_1^z$ ,  $ed F_2^z$  and  $ed F_3^z$  represent the driving force during the experiment.  $md F_1^z$ ,  $md F_2^z$  and  $md F_3^z$  represent the driving

force calculated in the existing literature.  ${}^{ea}F_{1z}^{dp}$ ,  ${}^{ea}F_{2z}^{dp}$  and  ${}^{ea}F_{3z}^{dp}$  represent the deviation percentage of the proposed method.  ${}^{ea}F_{1z}^{dp}$ ,  ${}^{ea}F_{2z}^{dp}$  and  ${}^{ea}F_{3z}^{dp}$  denote the deviation percentage in existing literature.

It can be seen from Figs. 7 to 8 that the experimental results are in good agreement with the simulation results, which proves the reliability of the analytical analysis method of driving force proposed.

- (1) The accuracy of inverse dynamic solution algorithm proposed in this paper is slightly higher than the existing algorithm in terms of maximum difference, error percentage and the average error value.
- (2) When using this method to design dynamic controller, the stability of the algorithm is better, which can improve the anti-interference and anti-noise performance of the system.
- (3) There is a certain deviation between the simulation value and the experiment value, which may be caused by the external uncertainty dynamic disturbance.

Set different posture alignment paths for experiment and compare the experimental value with the model value. It can be found that the maximum error percentage is less than 1.61% which is lower than the maximum value of the error percentage 1.98% in comparative literature [30].

## 7. Conclusions

An analytical modeling method of driving force of parallel posture alignment mechanism based on positioner is proposed. The following conclusions have been reached:

- (1) Based on independent variables in kinematics parameters, dynamic equations of each component are established by Newton–Euler method. Combining with the deformation compatibility equation, the force acting on the joint of the positioner and the moving platform are analyzed analytically, and then, the driving force is solved analytically.
- (2) The efficiency and accuracy of the algorithm is analyzed through simulation and experiment, respectively. It can be seen from the simulation and experiment results that the algorithm proposed in this paper is slightly better than the existing algorithm in the accuracy of driving force solution. The driving force solution time is reduced by 56.28% compared with the existing algorithm, which proves the validity and applicability of the modeling method.
- (3) The novelty of this paper is based on Newton–Euler method, combining the elastoplastic friction model and deformation coordination analysis, the dynamic modeling is carried out, and the driving force is analytically calculated through vector cross-product, which improve the efficiency of solving the driving force and ensuring the calculation accuracy.

The approach can be used for other robots than the one discussed in this article.

**Acknowledgements.** The authors would like to acknowledge the editors and the reviewers for their insightful comments.

**Author contributions.** Zhihao Wang completed the article writing, simulation analysis and experimental verification. Hongbin Li provided modification suggestions and financial support for the experiment. Nina Sun was responsible for paper polishing.

**Financial support.** This study was funded by National Natural Science Foundation of China (Grant No. 52075036), Shandong Provincial Natural Science Foundation (Grant No. ZR2022QE219) and Scientific Research Foundation for the introduction of talent of Ludong University (Grant No. 20210108). Hongbin Li is the principal investigator the fund 52075036 in Ludong University, and Zhihao Wang is the principal investigator of fund ZR2022QE219 and fund 20210108. Ludong University is the cooperative unit of the fund 52075036.

**Conflicts of interest.** The authors declare that they have no conflict of interest.

**Ethical approval.** Not applicable.

## References

- [1] H. L. Vieira, J. V. de Carvalho Fontes and M. M. da Silva, “Reliable redundancy resolution strategies for kinematically redundant parallel manipulators,” *Mech. Mach. Theory* **167**, 104531 (2022).
- [2] Y. Cho, J. Cheong, M. G. Kim, B.-J. Yi and W. Kim, “Efficient optimal force distribution method of the parallel mechanism with actuator redundancy based on geometric interpretation,” *J. Mech. Sci. Technol.* **33**(6), 2915–2928 (2019).
- [3] Z. Chen, L. Xu, W. Zhang and Q. Li, “Closed-form dynamic modeling and performance analysis of an over-constrained 2PUR-PSR parallel manipulator with parasitic motions,” *Nonlinear Dyn.* **96**(1), 517–534 (2019).
- [4] A. Arian, B. Danaei, H. Abdi and S. Nahavandi, “Kinematic and dynamic analysis of the Gantry-Tau, a 3-DoF translational parallel manipulator,” *Appl. Math. Model.* **51**, 217–231 (2017).
- [5] X. Chen and J. Guo, “Effects of spherical clearance joint on dynamics of redundant driving spatial parallel mechanism,” *Robotica* **39**(6), 1064–1080 (2021).
- [6] A. Hassani, S. Khalilpour, A. Bataleblu and H. D. Taghirad, “Full dynamic model of 3-UPU translational parallel manipulator for model-based control schemes,” *Robotica* **40**(8), 2815–2830 (2022).
- [7] X. Li, H. Sun, L. Liao and J. Song, “Establishing an improved kane dynamic model for the 7-DOF reconfigurable modular robot,” *Math. Probl. Eng.* **2017**, 1–13 (2017).
- [8] C. Qiu and J. S. Dai. *Analysis and Synthesis of Compliant Parallel Mechanisms - Screw Theory Approach* (Springer, London, 2020).
- [9] J. Jiao, Y. Wu, K. Yu and R. Zhao, “Dynamic modeling and experimental analyses of Stewart platform with flexible hinges,” *J. Vib. Control* **25**(1), 151–171 (2019).
- [10] Y. Jiang, T. Li and L. Wang, “The dynamic modeling, redundant-force optimization, and dynamic performance analyses of a parallel kinematic machine with actuation redundancy,” *Robotica* **33**(2), 241–263 (2015).
- [11] X. Chen, F. Dong and Q. Wang, “Dynamic equation of 4-ups-upu parallel mechanism based on Newton-Euler approach,” *Opt. Precis. Eng.* **23**(11), 3129–3137 (2015).
- [12] Z. Bi, W. Zhang, I.-M. Chen and S. Lang, “Automated generation of the D-H parameters for configuration design of modular manipulators,” *Robot. Comput.-Integr. Manuf.* **23**(5), 553–562 (2007).
- [13] T. Li, S. Jia and J. Wu, “Dynamic model of a 3-DOF redundantly actuated parallel manipulator,” *Int. J. Adv. Robot. Syst.* **13**(5), 1729881416662791 (2016).
- [14] L. Cao, A. T. Dolovich, A. L. Schwab, J. L. Herder and W. Zhang, “Toward a unified design approach for both compliant mechanisms and rigid-body mechanisms: Module optimization,” *J. Mech. Des.* **137**(12), 122301 (2015).
- [15] Y. Yang, Z. Q. Wang, Y. G. Kang and Z. P. Chang, “A Deformation Analysis and Compensation Algorithm for Bracket Structure of Automatic Drill-Riveting System,” *In: Advanced Materials Research*. vol. 912 (Trans Tech Publications, Switzerland, 2014) pp. 539–544.
- [16] C. Yang, Q. Li, Q. Chen and L. Xu, “Elastostatic stiffness modeling of overconstrained parallel manipulators,” *Mech. Mach. Theory* **122**, 58–74 (2018).
- [17] H. Wang, G. Liu, L. Wu and T. Zhang, “Modeling and parameter revising method of rigid-flexible coupling dynamics model,” *J. Coast. Res.* **73**(10073), 720–724 (2015).
- [18] X. Liu, Y. Xu, J. Yao, J. Xu, S. Wen and Y. Zhao, “Control-faced dynamics with deformation compatibility for a 5-DOF active over-constrained spatial parallel manipulator 6PUS-UPU,” *Mechatronics* **30**, 107–115 (2015).
- [19] Z. Wang, Y. Li, P. Sun, Y. Luo, B. Chen and W. Zhu, “A multi-objective approach for the trajectory planning of a 7-DOF serial-parallel hybrid humanoid arm,” *Mech. Mach. Theory* **165**, 104423 (2021).
- [20] S. Wen, H. Yu, B. Zhang, Y. Zhao, H.-K. Lam, G. Qin and H. Wang, “Fuzzy identification and delay compensation based on the force/position control scheme of the 5-DOF redundantly actuated parallel robot,” *Int. J. Fuzzy Syst.* **19**(1), 124–140 (2017).
- [21] H. Qu, C. Zhang and S. Guo, “Structural synthesis of a class of kinematically redundant parallel manipulators based on modified G–K criterion and RDOF criterion,” *Mech. Mach. Theory* **130**, 47–70 (2018).
- [22] J. Peng, W. Xu, Z. Hu, B. Liang and A. Wu, “Modeling and analysis of the multiple dynamic coupling effects of a dual-arm space robotic system,” *Robotica* **38**(11), 2060–2079 (2020).
- [23] Y. Liu, J. Li, Z. Zhang, X. Hu and W. Zhang, “Experimental comparison of five friction models on the same test-bed of the micro stick-slip motion system,” *Mech. Sci.* **6**(1), 15–28 (2015).
- [24] X. Liu, J. Yao, Q. Li and Y. Zhao, “Coordination dynamics and model-based neural network synchronous controls for redundantly full-actuated parallel manipulator,” *Mech. Mach. Theory* **160**, 104284 (2021).
- [25] R. C. Hibbeler. *Mechanics of Materials*. 8th edition (Prentice Hall, New Jersey, USA, 2006).
- [26] S. B. Niku. *Introduction to Robotics: Analysis, Control, Applications* (Prentice Hall, New Jersey, USA, 2020).
- [27] Y. Yang, J.-M. Qi, X.-H. Tang and Y.-Y. Gu, “Further results about traveling wave exact solutions of the (2+1)-dimensional modified KDV equation,” *Adv. Math. Phys.* **2019**, 1–10 (2019).
- [28] V. G. Martínez, L. H. Encinas, A. D. M. Muñoz and A. Q. Dios, “Using free mathematical software in engineering classes,” *Axioms* **10**(4), 253 (2021).
- [29] Q. Wang, W. Zhou, Y. Cheng, G. Ma, X. Chang, Y. Miao and E. Chen, “Regularized moving least-square method and regularized improved interpolating moving least-square method with nonsingular moment matrices,” *Appl. Math. Comput.* **325**, 120–145 (2018).
- [30] K. S. Stojanović and D. Mosić, “Generalization of the Moore–Penrose inverse,” *Revista de la Real Academia de Ciencias Exactas, Físicas y Naturales. Serie A. Matemáticas* **114**(4), 1–16 (2020).
- [31] Z. Wang, W. Chen, M. Wang, Q. Xu and C. Huang, “Kinematic calibration of bracket type parallel posture alignment mechanism considering the gravity effect,” *Ind. Robot* **46**(5), 581–598 (2019).

- [32] A. Castro, J. F. Martínez-Osuna, R. Michel, M. Escoto-Rodríguez, S. H. Bullock, A. Cueva, E. López-Reyes, J. Reimer, M. Salazar, S. Villarreal and Vargas R., “A low-cost modular data-acquisition system for monitoring biometeorological variables,” *Comput. Electron. Agric.* **141**, 357–371 (2017).
- [33] T. Sun, Y. Song, G. Dong, B. Lian and J. Liu, “Optimal design of a parallel mechanism with three rotational degrees of freedom,” *Robot. Comput.-Integr. Manuf.* **28**(4), 500–508 (2012).
- [34] A. Perrusquía, W. Yu and A. Soria, “Position/force control of robot manipulators using reinforcement learning,” *Ind. Robot* **46**(2), 267–280 (2019).
- [35] D. M. Tuan and P. D. Hieu, “Adaptive position/force control for robot manipulators using force and velocity observer,” *J. Electr. Eng. Technol.* **14**(6), 2575–2582 (2019).